

# One-Step Hydrothermal Synthesis of 2D Hexagonal Nanoplates of $\alpha$ -Fe<sub>2</sub>O<sub>3</sub>/Graphene Composites with Enhanced Photocatalytic Activity

Sancan Han, Linfeng Hu,\* Ziqi Liang, Swelm Wageh, Ahmed A. Al-Ghamdi, Yongsheng Chen, and Xiaosheng Fang\*

There has been significant progress in the field of semiconductor photocatalysis, but it is still a challenge to fabricate low-cost and high-activity photocatalysts because of safety issues and non-secondary pollution to the environment. Here, 2D hexagonal nanoplates of  $\alpha$ -Fe<sub>2</sub>O<sub>3</sub>/graphene composites with relatively good distribution are synthesized for the first time using a simple, one-step, template-free, hydrothermal method that achieves the effective reduction of the graphene oxide (GO) to graphene and intimate and large contact interfaces of the  $\alpha$ -Fe<sub>2</sub>O<sub>3</sub> nanoplates with graphene. The  $\alpha$ -Fe<sub>2</sub>O<sub>3</sub>/graphene composites showed significantly enhancement in the photocatalytic activity compared with the pure  $\alpha$ -Fe<sub>2</sub>O<sub>3</sub> nanoplates. At an optimal ratio of 5 wt% graphene, 98% of Rhodamine (RhB) is decomposed with 20 min of irradiation, and the rate constant of the composites is almost four times higher than that of pure  $\alpha$ -Fe<sub>2</sub>O<sub>3</sub> nanoplates. The decisive factors in improving the photocatalytic performance are the intimate and large contact interfaces between 2D hexagonal  $\alpha$ -Fe<sub>2</sub>O<sub>3</sub> nanoplates and graphene, in addition to the high electron withdrawing/storing ability and the high conductivity of reduced graphene oxide (RGO) formed during the hydrothermal reaction. The effective charge transfer from  $\alpha$ -Fe<sub>2</sub>O<sub>3</sub> nanoplates to graphene sheets is demonstrated by the significant weakening of photoluminescence in  $\alpha$ -Fe<sub>2</sub>O<sub>3</sub>/graphene composites.

non-toxicity and low cost. However, it notoriously suffers from poor conductivity, a short hole-diffusion length and high electron-hole recombination rate, which inhibit its promising applications in photocatalysis.<sup>[8–10]</sup> The main limitation is believed to be the difficult separation of electron-hole pairs and their easy recombination. To date, a variety of studies have been adopted to overcome these obstacles including metal and non-metal doping.<sup>[7,11,12]</sup> However, there has been limited success to greatly improve its photocatalytic properties.

Graphene could play an important role as the charge transfer medium, which slows the recombination of photo- or electrochemically generated electron-hole pairs, thus increasing charge transfer rate of electrons and surface adsorbed amount of chemical molecules through  $\pi$ - $\pi$  interaction.<sup>[13,14]</sup> More recently, TiO<sub>2</sub>/graphene composites have sparked much interest in effectively promoting transfer and separating photoinduced carriers for photocatalysis.<sup>[14–18]</sup> However, nanostructured carbons (activated carbon, carbon

nanotubes, and fullerenes) have seldom been found to improve the photocatalytic activity of  $\alpha$ -Fe<sub>2</sub>O<sub>3</sub>,<sup>[19]</sup> which explains why the  $\alpha$ -Fe<sub>2</sub>O<sub>3</sub>/graphene composites were only investigated in LIBs.<sup>[20–22]</sup> Graphene, as a rising star material and another allotrope of carbon, has many exceptional properties. Therefore, in comparison with other carbon allotropes, it is possible to improve

## 1. Introduction

$\alpha$ -Fe<sub>2</sub>O<sub>3</sub>, which has a favorable bandgap (1.9–2.2 eV), has been intensively investigated in lithium ion batteries (LIB),<sup>[1,2]</sup> field-effect transistors (FETs),<sup>[3]</sup> field emitters,<sup>[4]</sup> sensors,<sup>[5]</sup> pigments,<sup>[6]</sup> and catalysis<sup>[7]</sup> due to its chemical stability,

S. C. Han, Prof. L. F. Hu, Prof. Z. Q. Liang, Prof. X. S. Fang  
Department of Materials Science  
Fudan University  
Shanghai 200433, P. R. China  
E-mail: linfenghu@fudan.edu.cn; xshfang@fudan.edu.cn  
Dr. S. Wageh, Dr. A. A. Al-Ghamdi  
Department of Physics  
Faculty of Science, King Abdulaziz University  
Jeddah 21589, Saudi Arabia

DOI: 10.1002/adfm.201401279

Prof. Y. S. Chen  
Key Laboratory of Functional Polymer Materials and  
the Centre of Nanoscale Science and Technology  
Institute of Polymer Chemistry, College of Chemistry  
Nankai University  
Tianjin 300071, P. R. China



the photocatalytic performance in terms of the integration of  $\alpha$ -Fe<sub>2</sub>O<sub>3</sub> with graphene. Parida et al.<sup>[23]</sup> reported that  $\alpha$ -Fe<sub>2</sub>O<sub>3</sub> nanorod/reduced graphene oxide (RGO) composites showed relatively enhanced photocatalytic efficiency for phenol degradation and Li et al.<sup>[24]</sup> reported the photodegradation of toluene over a spindle-shaped  $\alpha$ -Fe<sub>2</sub>O<sub>3</sub>/graphene composite improved due to the fast transfer of photogenerated electrons from  $\alpha$ -Fe<sub>2</sub>O<sub>3</sub> to the RGO sheets. These renewed efforts revealed that  $\alpha$ -Fe<sub>2</sub>O<sub>3</sub>/graphene composites were truly different from other  $\alpha$ -Fe<sub>2</sub>O<sub>3</sub>/carbon composites on enhancement of photocatalytic activity for the degradation of organic pollutants, showing the promising potential for photocatalysis. However, the agglomeration of the obtained samples was very serious, inhibiting the contact between RGO and  $\alpha$ -Fe<sub>2</sub>O<sub>3</sub>, which was responsible for unsatisfactory transport of photoinduced electrons from  $\alpha$ -Fe<sub>2</sub>O<sub>3</sub> to RGO sheet and thus drastically decreased photocatalytic activity. Therefore, the synthesis of  $\alpha$ -Fe<sub>2</sub>O<sub>3</sub>/graphene composites with good distribution and enhanced photocatalytic activity is desirable for practical applications.

2D nanomaterials, which have a surface area that is dominated by one specific crystallographic plane, have received increasing interest in decades.<sup>[25,26]</sup> Since a 2D material is entirely made up of its surface, the interface between the surface and the substrate and the presence of adatoms can dramatically alter the material's properties.<sup>[27]</sup> The unique surface structure can guarantee the intimate and large contact interfaces with graphene, which favors the transfer of photogenerated electrons from the semiconductor to graphene, leading to the higher efficiency in the separation of photogenerated charge carriers and a higher photoactivity.<sup>[28]</sup> Here, 2D  $\alpha$ -Fe<sub>2</sub>O<sub>3</sub> hexagonal nanoplates/graphene composites with good distribution are synthesized for the first time using a simple one-step template-free hydrothermal method, which achieves the effective reduction of the graphene oxide (GO) to graphene and the intimate and large contact interfaces of the  $\alpha$ -Fe<sub>2</sub>O<sub>3</sub> nanoplates with graphene. The  $\alpha$ -Fe<sub>2</sub>O<sub>3</sub>/graphene composites with different weight ratios of GO to  $\alpha$ -Fe<sub>2</sub>O<sub>3</sub> (0.1%:1, 1.0%:1, 2.0%:1, 5.0%:1, 8.0%:1) are synthesized and are defined as 0.1GRF, 1.0GRF, 2.0GRF, 5.0GRF, and 8.0GRF, respectively, and the pure  $\alpha$ -Fe<sub>2</sub>O<sub>3</sub> nanoplates were used for comparison. The significant increase in photocatalytic activity is confirmed by the degradation of Rhodamine B (RhB) in the presence of the  $\alpha$ -Fe<sub>2</sub>O<sub>3</sub>/graphene composites, and the rate constant  $k_a$  of 5.0GRF reaches 0.19489, exceeding that of pure  $\alpha$ -Fe<sub>2</sub>O<sub>3</sub> by a factor of four. It is also worth noting that 98% of RhB was degraded for 5.0GRF in 20 min, which is one of the most effective photocatalysts to our knowledge. Furthermore, this work highlights the mechanism for enhancing photocatalytic performance after the introduction of GO, which is beneficial for further improving photoactivity.

## 2. Result and Discussion

The phases of the Fe<sub>2</sub>O<sub>3</sub>/GO composites with different weight addition ratios of GO were investigated by X-ray diffraction (XRD), as shown in Figure 1. All the diffraction peaks are indexed to hexagonal iron oxide structure (JCPDS card No. 33-0664) with the lattice parameters of  $a = b = 0.50356$  nm,

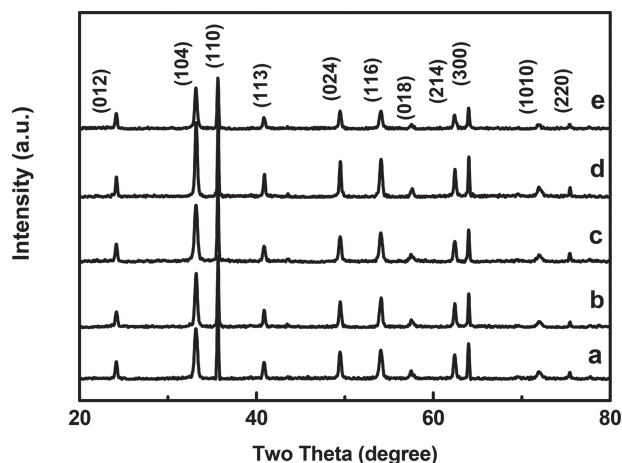


**Figure 1.** XRD patterns of the obtained  $\alpha$ -Fe<sub>2</sub>O<sub>3</sub>/GO composites: a) 0.1GRF, b) 1.0GRF, c) 2.0GRF, d) 5.0GRF, and e) 8.0GRF.

$c = 1.37489$  nm, and no peak shift was observed when GO was introduced into the  $\alpha$ -Fe<sub>2</sub>O<sub>3</sub> nanoplates, meaning that the formation of the composites with the present weight ratios of GO has a negligible effect on the crystal phase of  $\alpha$ -Fe<sub>2</sub>O<sub>3</sub> nanoplates. The peaks at  $2\theta$  values at 24.2°, 33.2°, 35.5°, 40.9°, 49.5°, 54.1°, 57.6°, 62.2°, 64.2°, 72.0°, 75.3° can be indexed to (012), (104), (110), (113), (024), (116), (018), (214), (300), (1010), and (220) crystal planes of hexagonal iron oxide, respectively. The strong and sharp diffraction peaks showed that the obtained products were well crystallized. Similar to the previous TiO<sub>2</sub>/graphene composites using GO as the precursor of graphene,<sup>[18]</sup> no typical diffraction peaks of GO were detected, which can be explained by 1) the small amount of GO in the  $\alpha$ -Fe<sub>2</sub>O<sub>3</sub>/GO composites and 2) the destroyed regular stack of GO by the intercalation of  $\alpha$ -Fe<sub>2</sub>O<sub>3</sub>.

Figure 2 shows the scanning electron microscopy (SEM) and transmission electron microscopy (TEM) images of pure hexagonal  $\alpha$ -Fe<sub>2</sub>O<sub>3</sub> nanoplates and  $\alpha$ -Fe<sub>2</sub>O<sub>3</sub>/GO composites. As shown in Figure 2a–c, the hexagonal  $\alpha$ -Fe<sub>2</sub>O<sub>3</sub> nanoplates with good size distribution were formed with the width of about 200 nm. In Figure 2c, the well defined hexagonal  $\alpha$ -Fe<sub>2</sub>O<sub>3</sub> nanoplate was observed, the high-resolution TEM (HRTEM) image in the inset of the right corner from the white square shows the distinguishable lattice spacing is 0.25 nm, corresponding to the (110) plane of  $\alpha$ -Fe<sub>2</sub>O<sub>3</sub>, which is consistent with the XRD results. In Figure 2d, through the transparent GO,  $\alpha$ -Fe<sub>2</sub>O<sub>3</sub> nanoplates, which are lying horizontally (white square) or standing vertically (black square), are randomly dispersed on the GO nanosheets. Even after a long duration of sonication during the preparation of the TEM specimen, the GO nanosheets still act as stable supporting materials for anchoring  $\alpha$ -Fe<sub>2</sub>O<sub>3</sub> nanoplates, implying a strong interaction between GO and  $\alpha$ -Fe<sub>2</sub>O<sub>3</sub> nanoplates. Most carboxyl and hydroxyl groups, which can act as anchor sites, are decorated on the edges of GO, leading to in situ formation of  $\alpha$ -Fe<sub>2</sub>O<sub>3</sub> nanoparticles (NPs) attached on the edges of GO sheets.<sup>[29]</sup> Similar to the dopamine molecule, GO has a large quantity of phenolic hydroxyl groups that can coordinate with  $\alpha$ -Fe<sub>2</sub>O<sub>3</sub> nanoplates.<sup>[30]</sup> Hence,  $\alpha$ -Fe<sub>2</sub>O<sub>3</sub> nanoplates could be located in the entire GO sheet because of the coordination between phenolic hydroxyls and  $\alpha$ -Fe<sub>2</sub>O<sub>3</sub>, which is in

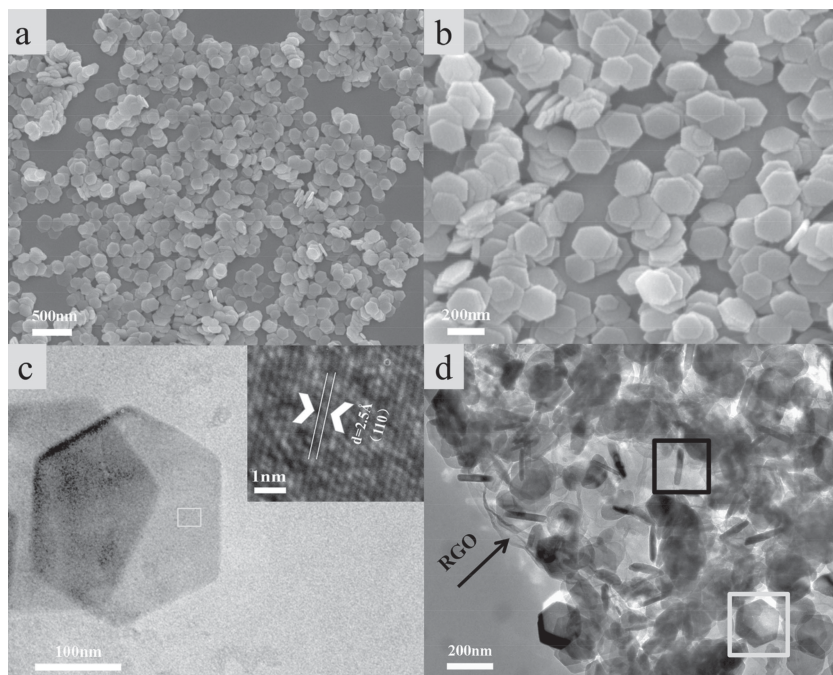


**Figure 2.** SEM and TEM images of  $\alpha$ -Fe<sub>2</sub>O<sub>3</sub> hexagonal nanoplates and  $\alpha$ -Fe<sub>2</sub>O<sub>3</sub>/GO composites. a,b) SEM images of pure hexagonal  $\alpha$ -Fe<sub>2</sub>O<sub>3</sub> nanoplates. c) TEM image of single hexagonal  $\alpha$ -Fe<sub>2</sub>O<sub>3</sub> nanoplate and HRTEM image from the white square. d) TEM image of  $\alpha$ -Fe<sub>2</sub>O<sub>3</sub>/GO composites.

accordance with our TEM observations. The detailed structure information of the hexagonal  $\alpha$ -Fe<sub>2</sub>O<sub>3</sub> nanoplate was investigated by the atomic force microscopy (AFM), which accurately shows the thickness and width of the  $\alpha$ -Fe<sub>2</sub>O<sub>3</sub> nanoplates. As shown in **Figure 3a,b**, the tapping-mode AFM images and the height cross-sectional profiles of hexagonal  $\alpha$ -Fe<sub>2</sub>O<sub>3</sub> nanoplates on a mica substrate were obtained, demonstrating that the thickness of the  $\alpha$ -Fe<sub>2</sub>O<sub>3</sub> nanoplate is about 15.4 nm and the width of the  $\alpha$ -Fe<sub>2</sub>O<sub>3</sub> nanoplate is about 197.6 nm, in agreement with the above mentioned data. Moreover, the AFM images and the height cross-sectional profiles confirmed the surface of  $\alpha$ -Fe<sub>2</sub>O<sub>3</sub> nanoplate was quite smooth, suggesting the well-defined feature of the sample. The aspect ratio is about 0.078, which is significantly small. The carboxylic anions have strong chelating ability to transition metal ions, thus the presence of sodium acetate could coordinate with hematite nanocrystals on (001) planes and retard the growth along the [001] direction and promote the growth along the *ab*-plane in the growth medium,<sup>[31]</sup> therefore explaining the small aspect ratio of  $\alpha$ -Fe<sub>2</sub>O<sub>3</sub> nanoplates. Standard and thin hexagonal nanoplate can be easily observed in **Figure 3c**.

Fourier transform infrared (FT-IR) spectroscopy was used to investigate the chemical structure and their changes of the pure GO and  $\alpha$ -Fe<sub>2</sub>O<sub>3</sub>/GO composites. As shown in **Figure 4a**, the FT-IR spectrum of GO exhibits the C=O and C-O stretching vibration band of COOH groups are at  $\approx 1742$  cm<sup>-1</sup> and  $\approx 1045$  cm<sup>-1</sup>,<sup>[32]</sup> respectively, and a broad band at  $\approx 3417$  cm<sup>-1</sup> is assigned to hydroxyl groups, indicating the sufficiently oxidized GO with hydroxyl and carboxyl groups.<sup>[30]</sup> The characteristic peak for the aromatic C=C is at  $\approx 1619$  cm<sup>-1</sup>. In comparison, the  $\alpha$ -Fe<sub>2</sub>O<sub>3</sub>/GO composites show almost the same peaks, but the positions

of the bands are slightly blue shifted and the sharpness of the peaks is changed, indicating the change in the coordination environment of various functional groups in  $\alpha$ -Fe<sub>2</sub>O<sub>3</sub>/GO composites. In particular, the peaks at  $\approx 1742$  cm<sup>-1</sup> and  $\approx 3417$  cm<sup>-1</sup>, corresponding to stretching vibration band of carboxyl and hydroxyl group, respectively, were much weaker than those of pure GO, indicating that the oxygen functional groups on GO are partly removed and that the reduced GO still contains some oxygen containing functionalities, which can induce secondary interactions of RGO with  $\alpha$ -Fe<sub>2</sub>O<sub>3</sub>.<sup>[33]</sup>

The photocatalytic activity of  $\alpha$ -Fe<sub>2</sub>O<sub>3</sub>/graphene composites was evaluated by the degradation of RhB (10 mg/L) in the presence of H<sub>2</sub>O<sub>2</sub> under Xe light irradiation (350 W). As shown in **Figure 5a**, the photocatalytic degradation of RhB was monitored through the change in intensity of the characteristic absorption peak at 550 nm, showing that the absorption peak decreased in intensity as the time prolonged. The variation of the degree of degradation (*c/c*<sub>0</sub>) with the time of irradiation for  $\alpha$ -Fe<sub>2</sub>O<sub>3</sub> and  $\alpha$ -Fe<sub>2</sub>O<sub>3</sub>/graphene composites is plotted in **Figure 5b**. The degrees of the degradation for the

$\alpha$ -Fe<sub>2</sub>O<sub>3</sub>/graphene composites were all significantly higher than that of pure  $\alpha$ -Fe<sub>2</sub>O<sub>3</sub>. With an increase in the mass ratios of GO, the photodegradation performance of  $\alpha$ -Fe<sub>2</sub>O<sub>3</sub>/graphene composites showed the increasing trend. However, the photoactivity performances of 5.0GRF and 8.0GRF were almost the same, except for slight difference in the first 20 minutes. **Figure 5c** displayed that the degree of RhB degradation for 5.0GRF reached 98%, while that for 8.0GRF was 95% in 20 min irradiation, showing that more graphene in the system does not always guarantee the best result in photocatalytic application. The highest photocatalytic activity was obtained for composites prepared with 0.5 wt.% of GO. According to the previous studies, the photodegradation of RhB can be considered as a pseudo-first order reaction,<sup>[34,35]</sup> when *c*<sub>0</sub> is small enough, the photocatalytic reaction kinetics can be expressed as follows:

$$\ln(c_0/c) = k_a t$$

where *k*<sub>a</sub> is the degradation rate constant and *c*<sub>0</sub> and *c* are the initial concentration and the concentration at a reaction time *t*, respectively. The rate constant *k*<sub>a</sub> is the basic kinetic parameter for the different photocatalysts, reflecting the reaction rate of a photocatalytic process, thus the variations in the form of ln(*c*<sub>0</sub>/*c*) as a function of irradiation time are displayed in **Figure 5d**. According to the kinetic curves, the 5.0GRF composites have the highest rate constant of *k*<sub>a</sub> = 0.19489 min<sup>-1</sup>, which is almost four times higher than that of pure  $\alpha$ -Fe<sub>2</sub>O<sub>3</sub>. The rate constants follow the order: 5.0GRF (0.19489 min<sup>-1</sup>) > 8.0GRF (0.16714 min<sup>-1</sup>) > 2.0GRF (0.14101 min<sup>-1</sup>) > 1.0GRF (0.11486 min<sup>-1</sup>) > 0.1GRF (0.0748 min<sup>-1</sup>) >  $\alpha$ -Fe<sub>2</sub>O<sub>3</sub> (0.05572 min<sup>-1</sup>). These results in photocatalytic performance allow us to conclude that the

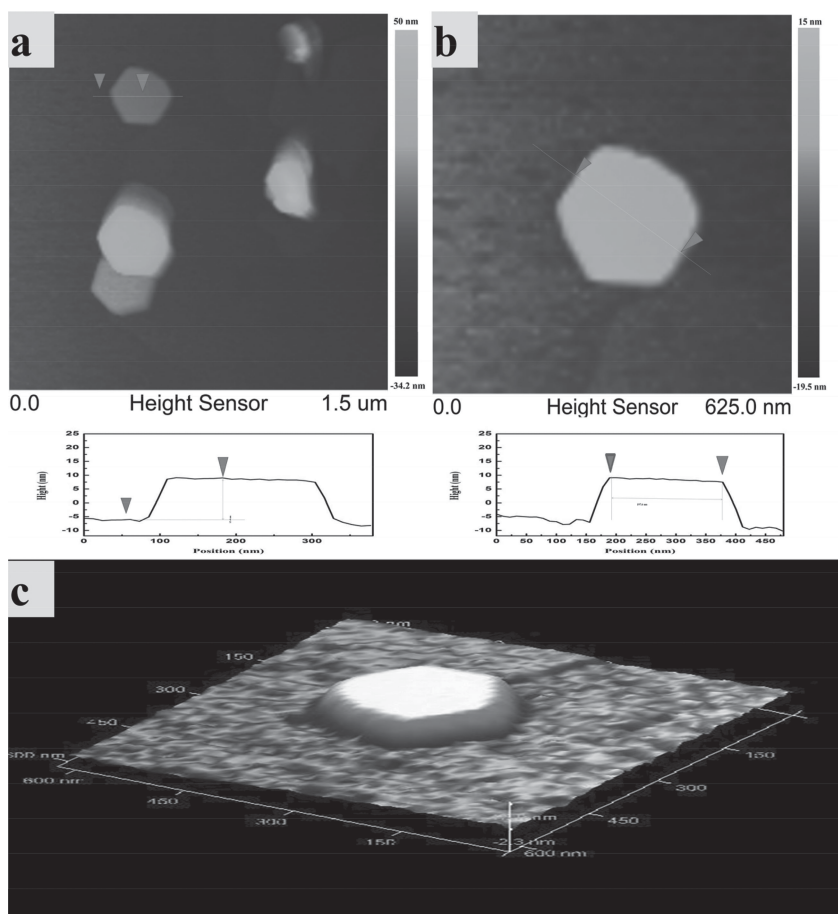


**Figure 3.** a,b) Tapping-mode AFM images (top) and the height cross-sectional profiles (middle) of pure  $\alpha$ -Fe<sub>2</sub>O<sub>3</sub> nanoplates on a mica substrate. The thickness of  $\alpha$ -Fe<sub>2</sub>O<sub>3</sub> nanoplate is 15.4 nm and the width of  $\alpha$ -Fe<sub>2</sub>O<sub>3</sub> nanoplate is 197.6 nm. c) 3D AFM images of single hexagonal  $\alpha$ -Fe<sub>2</sub>O<sub>3</sub> nanoplates.

presence of graphene is more efficient for increasing the photoactivity, and controlling the addition ratios of graphene in order to achieve an optimal synergistic interaction between graphene and  $\alpha$ -Fe<sub>2</sub>O<sub>3</sub>, which is important for the achievement in the

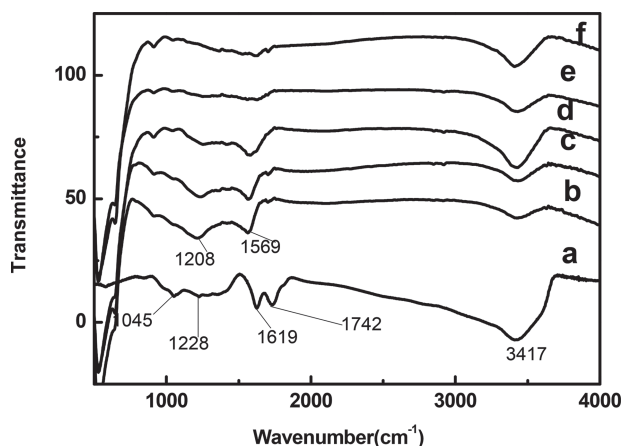


**Figure 4.** FT-IR transmittance spectra of GO and  $\alpha$ -Fe<sub>2</sub>O<sub>3</sub>/graphene composites: a) GO, b) 8.0GRF, c) 5.0GRF, d) 2.0GRF, e) 1.0GRF, and f) 0.1GRF.

best photoactivity of  $\alpha$ -Fe<sub>2</sub>O<sub>3</sub>/graphene nanocomposites.<sup>[16,36,37]</sup> The photocatalytic activity of semiconductor oxides is known to be mainly governed by light-absorption, surface area and the recombination rate of photogenerated charge carriers, etc.<sup>[15,38]</sup> It remains a significant challenge to distinguish which factor(s) dominate the photocatalytic activity in our system, and it is therefore important to address these problems comprehensively. Herein, the dominant factors have been discussed as follows.

The optical absorption properties of the different catalysts were investigated by the comparison of the UV-vis diffuse reflectance spectra (DRS), as shown in **Figure 6**. The combination of graphene with  $\alpha$ -Fe<sub>2</sub>O<sub>3</sub> nanoplates induced the change of the optical absorption. The absorption background of  $\alpha$ -Fe<sub>2</sub>O<sub>3</sub>/graphene composites decreased with the increasing mass contents of graphene because more graphene was formed onto the  $\alpha$ -Fe<sub>2</sub>O<sub>3</sub> nanoplates, which should be ascribed to the opacity of graphene.<sup>[39]</sup> That means the presence of graphene directly weakens the optical absorption properties, which has a negative effect on the photocatalytic performance.

In general, a larger surface area could offer more active adsorption sites that are catalytically active, which means the higher surface area will result in the higher photocatalytic activity. Nitrogen adsorption/desorption isotherms were used to investigate the specific surface area and pore size distribution of the obtained pure  $\alpha$ -Fe<sub>2</sub>O<sub>3</sub> and  $\alpha$ -Fe<sub>2</sub>O<sub>3</sub>/graphene composites. In **Table 1**, after introducing a small amount of graphene, the specific surface area of  $\alpha$ -Fe<sub>2</sub>O<sub>3</sub>/graphene composites decreases with the increasing graphene content. The slight decrease of surface area should be attributed to that the graphene coated on the surface of  $\alpha$ -Fe<sub>2</sub>O<sub>3</sub> nanoplates and blocked some mesopores and micropores. A further increase in graphene content higher than 2.0 wt%, the surface area shows an increased tendency with the increasing graphene content, which may be ascribed to the exfoliation and cross-linking point between graphene and  $\alpha$ -Fe<sub>2</sub>O<sub>3</sub> nanoplates.<sup>[23,33]</sup> However, the variation in the surface area of the different products is extremely limited, and the contribution from graphene to the specific surface area is negligible. To conclude, the surface area has no significant influence on the improvement of the photocatalytic performance. The change of pure  $\alpha$ -Fe<sub>2</sub>O<sub>3</sub> and  $\alpha$ -Fe<sub>2</sub>O<sub>3</sub>/graphene composites in the pore volume and pore diameter was irregular, indicating the  $\alpha$ -Fe<sub>2</sub>O<sub>3</sub> nanoplates are not uniformly distributed on the graphene, which is consistent with the TEM observations.

**Figure 7** shows a comparison of the Raman spectra of GO and 5.0GRF. In the case of GO, the two peaks observed at  $\sim$ 1339.8 cm<sup>-1</sup> and  $\sim$ 1598.3 cm<sup>-1</sup>, corresponding to the

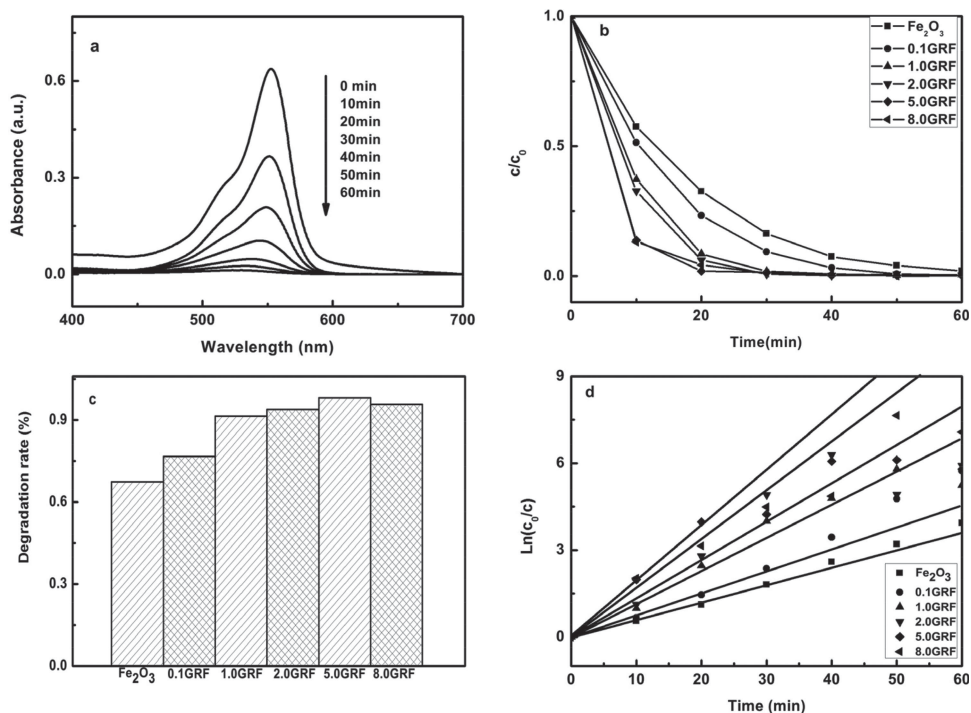


**Figure 5.** a) Time-dependent UV-vis absorption spectra in the presence of  $\alpha$ -Fe<sub>2</sub>O<sub>3</sub> under Xe light irradiation. b) Photodegradation of RhB by  $\alpha$ -Fe<sub>2</sub>O<sub>3</sub> and  $\alpha$ -Fe<sub>2</sub>O<sub>3</sub>/graphene composites under Xe light irradiation 60 min. c) Comparison of photocatalytic performance of  $\alpha$ -Fe<sub>2</sub>O<sub>3</sub> and  $\alpha$ -Fe<sub>2</sub>O<sub>3</sub>/graphene composites in 20 min. d) Kinetic curves of the degradation of RhB by  $\alpha$ -Fe<sub>2</sub>O<sub>3</sub> and  $\alpha$ -Fe<sub>2</sub>O<sub>3</sub>/graphene composites.

disorder band associated with structural defects created in graphene (D band) and well ordered scattering of the E<sub>2g</sub> phonon of sp<sup>2</sup> C atoms of graphene (G band), respectively.<sup>[15]</sup> The intensity of D band is stronger than that of G band, meaning the presence of high density of defects and structure disorder in GO. For the  $\alpha$ -Fe<sub>2</sub>O<sub>3</sub>/graphene composites (0.05:1), the two characteristic peaks at about 1321.0 (D band) and 1598.3 cm<sup>-1</sup> (G band) can be observed, suggesting the structure of graphene is maintained in the composite. The shifting in the D band position of  $\alpha$ -Fe<sub>2</sub>O<sub>3</sub>/graphene composite towards lower frequency by  $\approx 27$  cm<sup>-1</sup> compared with

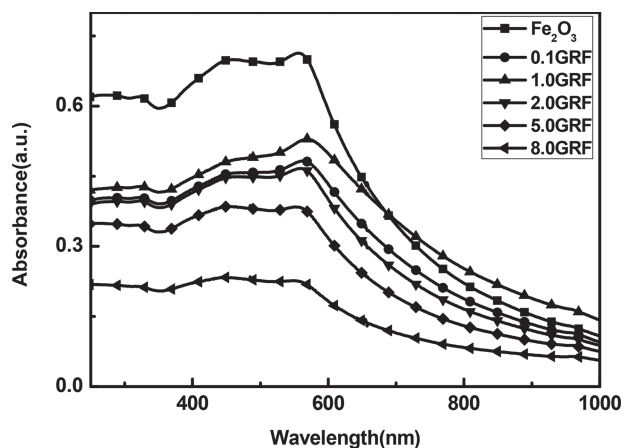


**Figure 6.** The UV-vis absorption spectra for the obtained pure  $\alpha$ -Fe<sub>2</sub>O<sub>3</sub> and  $\alpha$ -Fe<sub>2</sub>O<sub>3</sub>/graphene composites.

GO and all the fundamental Raman vibrations of  $\alpha$ -Fe<sub>2</sub>O<sub>3</sub> (black square:  $\approx 225$  cm<sup>-1</sup> corresponds to A<sub>1g</sub> symmetry;  $\approx 297$ ,  $\approx 413$ , and  $\approx 600$  cm<sup>-1</sup> for E<sub>g</sub> symmetry, respectively) suggest the combination of  $\alpha$ -Fe<sub>2</sub>O<sub>3</sub> nanoplates with the graphene layer. In addition, an increased D/G intensity ratio from 1.15 to 1.76 is also observed in comparison with that of pure GO, suggesting a decrease in the average size of the sp<sup>2</sup> domains during the hydrothermal process which confirms the reduction of GO to RGO.<sup>[23]</sup> The efficient reduction of GO to RGO after the hydrothermal treatment can also be evidenced by the comparison of XPS. **Figure 8** displays the comparison of the high-resolution C 1s XPS spectra of the GO and 5.0GRF. In **Figure 8a**, the C 1s spectrum of pure GO can be fitted into three peaks located at  $\approx 284.5$ ,  $\approx 286.6$  and  $\approx 287.7$  eV, which were assigned to C–C, C–OH, and C=O, respectively.<sup>[1]</sup> In comparison, the peak for C=O in the 5.0GRF is almost vanished, while still containing some oxygenated groups, implying that GO was substantially reduced after the hydrothermal reaction, which will enhance the conductivity of GO sheets. According to the mechanism by Hoffman et al.,<sup>[30,41]</sup> the higher conductivity leads to more effective charge separation and more effective antirecombination during photocatalytic process, thus improve the photocatalytic efficiency in the  $\alpha$ -Fe<sub>2</sub>O<sub>3</sub>/graphene composite system.

The efficiency of the photocatalytic process is measured by quantum yield ( $\Phi$ ), which is defined as the number of photons absorbed in Graphene-based composites can capture photoinduced electrons originated from  $\alpha$ -Fe<sub>2</sub>O<sub>3</sub> (or other semiconductor) particles.<sup>[40,41]</sup> In an ideal system,  $\Phi$  follows a simple relationship:

**Table 1.** BET surface area and pore size for the obtained pure  $\alpha$ -Fe<sub>2</sub>O<sub>3</sub> nanoplates and  $\alpha$ -Fe<sub>2</sub>O<sub>3</sub>/graphene composites.

Samples	Surface area [m <sup>2</sup> /g]	Pore volume [cm <sup>3</sup> /g]	Pore diameter [nm]
$\alpha$ -Fe <sub>2</sub> O <sub>3</sub>	23.545	0.147	19.493
0.1GRF	20.406	0.153	29.947
1.0GRF	22.061	0.120	21.769
2.0GRF	28.393	0.145	20.423
5.0GRF	28.818	0.119	16.448
8.0GRF	37.614	0.198	21.040

$$\Phi \propto k_{ct} / (k_{ct} + k_r)$$

where  $k_{ct}$  is the rate of the charge transfer processes and  $k_r$  indicates the electron-hole recombination rate. The above equation reveals that preventing the electron-hole recombination of semiconductor under illumination would be critical for the improvement of the quantum yield.<sup>[40,42]</sup> Hence, to understand the cause of the improvement in the photoactivity, the study in the transportation of photogenerated electrons and holes is of importance. Photoluminescence (PL) spectra is a well known technique to study transfer process of the interface charge carrier as well as the recombination process involving the electron-hole pairs in semiconductor particles,<sup>[43–45]</sup> and PL emission results from the radiative recombination of excited electrons and holes. As shown in **Figure 9**, the pure  $\alpha$ -Fe<sub>2</sub>O<sub>3</sub> nanoplates displayed a strong PL intensity, meaning the high recombination of charge carriers in pure  $\alpha$ -Fe<sub>2</sub>O<sub>3</sub> nanoplates. After the RGO is combined with the  $\alpha$ -Fe<sub>2</sub>O<sub>3</sub> nanoplates, the PL intensity of the  $\alpha$ -Fe<sub>2</sub>O<sub>3</sub>/graphene composites decreased with the increasing mass ratios of RGO, indicating that the recombination of photogenerated electron-hole pairs is efficiently hampered. Indeed, the RGO possesses the high electron withdrawing/storing ability and the high conductivity compared to GO, which can facilitate the charge separation, are beneficial to the photocatalytic performance.<sup>[46,47]</sup> Furthermore, the intimate and large contact interfaces with graphene have also improved

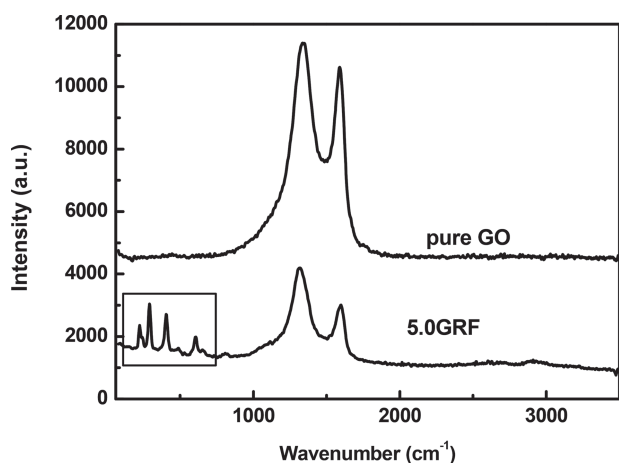


**Figure 7.** Raman spectra of graphene oxide (GO) and  $\alpha$ -Fe<sub>2</sub>O<sub>3</sub>/graphene composites with a loading of 5 wt% GO (5.0GRF).

the lifetime and transfer of photogenerated charge carriers. Based on the PL results, the intensity of 8.0GRF is weaker than that of 5.0GRF, meaning the better separation of photogenerated charge carriers; however, the efficiency of the photodegradation is lower than that of 5.0GRF, which is attributed to the lower light absorption discussed previously.

On the basis of the above discussion, the intimate and large contact interfaces between 2D hexagonal  $\alpha$ -Fe<sub>2</sub>O<sub>3</sub> nanoplates and graphene, and the high conductivity of RGO during the hydrothermal reaction, which would induce better transfer and the longer lifetime of photogenerated charge carriers, are the decisive factors to improve the photocatalytic performance. Accordingly, a possible reaction mechanism has been proposed, as illustrated in **Scheme 1**. The electrons in the valence band can be excited to the conduction band with the same amount of positively charged holes left to form electron-hole pairs when the UV-vis light irradiates, the electrons can then be transferred to the surface of graphene. The effective charge transfer can decrease the electron-hole pair recombination rate and prolong the lifetime of charge carriers, which increases the photocatalytic efficiency. The photoinduced electrons are apt to react with absorbed O<sub>2</sub> to form superoxide anion radical ( $\cdot$ O<sub>2</sub><sup>-</sup>), while the

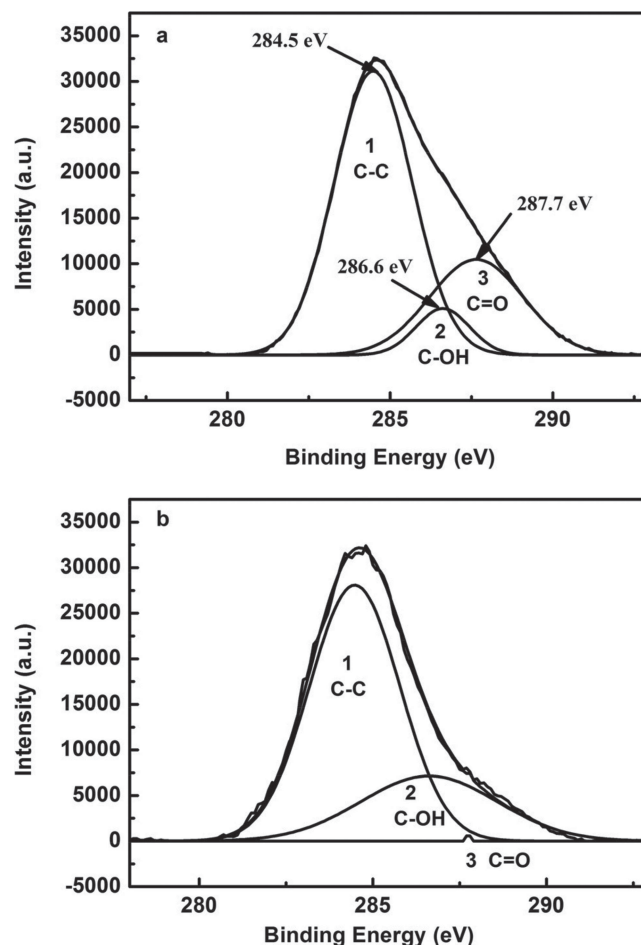


**Figure 8.** Peak deconvolution in C 1s of XPS spectrum: a) graphene oxide (GO) and b)  $\alpha$ -Fe<sub>2</sub>O<sub>3</sub>/graphene composites with a loading of 5 wt% GO (5.0GRF).

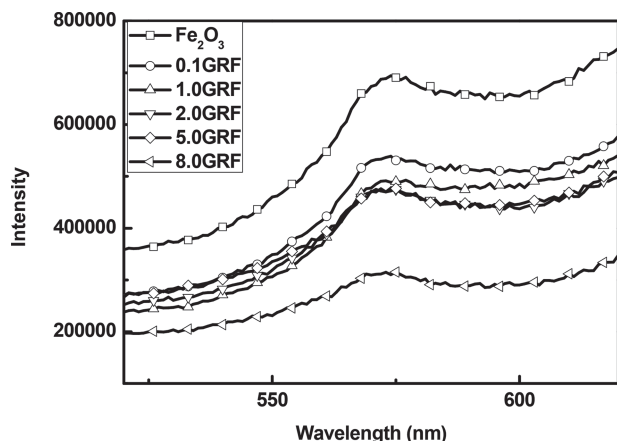
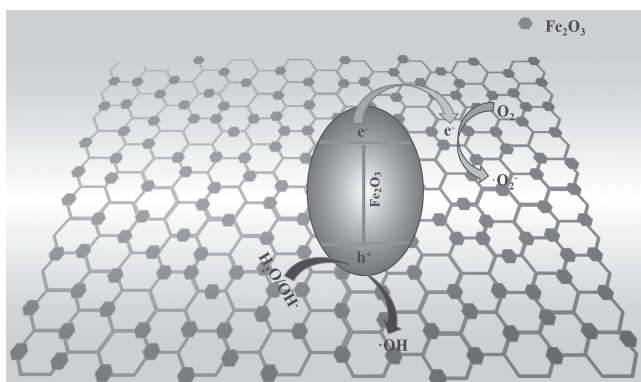
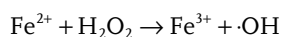
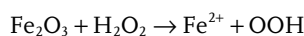
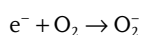
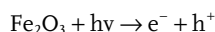


**Figure 9.** Photoluminescence spectra of the obtained pure  $\alpha$ - $\text{Fe}_2\text{O}_3$  and  $\alpha$ - $\text{Fe}_2\text{O}_3$ /graphene composites.

holes could also react with surface-bound  $\text{H}_2\text{O}$  and  $\text{OH}^-$  to produce hydroxy radicals ( $\cdot\text{OH}$ ). It is evident that hydroxy radicals were the main active species for the degradation of organic chemicals.<sup>[35,48]</sup> In our  $\alpha$ - $\text{Fe}_2\text{O}_3$ /graphene composite system, the photo-Fenton catalytic process is complex, other than the above fundamental photocatalytic reactions, the reactions between iron ion and  $\text{H}_2\text{O}_2$  are proceeding at the same time. At first,  $\text{Fe}^{3+}$  was reduced to  $\text{Fe}^{2+}$ . Subsequently,  $\text{Fe}^{2+}$  would react with  $\text{H}_2\text{O}_2$  to produce  $\cdot\text{OH}$  and  $\text{Fe}^{3+}$ , which can be regenerated to compete the  $\text{Fe}^{3+}/\text{Fe}^{2+}$  cycle to form more strong oxidant  $\cdot\text{OH}$  for the degradation of RhB.<sup>[49,50]</sup> In conclusion, the photocatalytic reaction of the  $\alpha$ - $\text{Fe}_2\text{O}_3$ /graphene composites in our system can be thus expressed as follows:



**Scheme 1.** The mechanism illustration of high photocatalytic activity for  $\alpha$ - $\text{Fe}_2\text{O}_3$ /graphene composites.

### 3. Conclusions

We have succeeded in preparing 2D  $\alpha$ - $\text{Fe}_2\text{O}_3$  hexagonal nanoplates/graphene composites with different weight ratios of GO to  $\alpha$ - $\text{Fe}_2\text{O}_3$  (0.1%:1, 1.0%:1, 2.0%:1, 5.0%:1, 8.0%:1) using a simple, one-step, template-free, hydrothermal method.  $\alpha$ - $\text{Fe}_2\text{O}_3$  hexagonal nanoplates were well-dispersed on the graphene, which is beneficial to the effective charge transfer from  $\alpha$ - $\text{Fe}_2\text{O}_3$  to graphene. The effect of different addition ratios of graphene on the photocatalytic activity of  $\alpha$ - $\text{Fe}_2\text{O}_3$ /graphene was systematically investigated, and the photocatalytic performance of the composites was discussed with respect to the light-absorbance properties, interaction between  $\alpha$ - $\text{Fe}_2\text{O}_3$  nanoplates and graphene, and the photoluminescence spectra. The intimate and large contact interfaces favor the effective charge transfer, leading to the higher photocatalytic activity of the  $\alpha$ - $\text{Fe}_2\text{O}_3$ /graphene. In terms of the safety and the non-secondary pollution to the environment, our composites are high-performance nanoscale photocatalysts. These composites with high photocatalytic activity could be beneficial to industrial applications to eliminate the organic pollutants from waste water.

### 4. Experimental Section

Graphene oxide was prepared by using a modified Hummers method<sup>[51]</sup> and following the previous publication.<sup>[52]</sup> Briefly, 5 g of flake graphite (average particle diameter of 4  $\mu\text{m}$ , 99.95% purity, Qingdao Tianhe Graphite Co. Ltd., Qingdao, China) and 3.75 g of  $\text{NaNO}_3$  (A.R.) were placed in a flask. Then, 375 mL of  $\text{H}_2\text{SO}_4$  (A.R.) was added with stirring in an ice-water bath, and 22.5 g of  $\text{KMnO}_4$  (A.R.) were slowly added over about 1 h. Stirring was continued for 2 h in the ice-water bath. After the mixture was stirred vigorously for 5 days at room temperature, 700 mL of 5 wt%  $\text{H}_2\text{SO}_4$  aqueous solution was added over about 1 h with stirring, and the temperature was kept at 98  $^\circ\text{C}$ . The resultant mixture was further stirred for 2 h at 98  $^\circ\text{C}$ . The temperature was reduced to 60  $^\circ\text{C}$ , 15 mL of  $\text{H}_2\text{O}_2$  (30 wt% aqueous solution) was added, and the mixture was stirred for 2 h at room temperature. To remove the ions of oxidant and other inorganic impurity, the resultant mixture was purified by repeating the following procedure cycle 15 times: centrifugation, removal of the supernatant liquid, addition of 2 L of a mixed aqueous solution of 3 wt%  $\text{H}_2\text{SO}_4$ /0.5 wt%  $\text{H}_2\text{O}_2$  to the bottom solid, and dispersing the solid using vigorous stirring and bath ultrasonication for 30 min at a power of 140 W. Then a similar procedure was repeated: three times using 3 wt%  $\text{HCl}$  aqueous solution (2 L) and one time using  $\text{H}_2\text{O}$  (2 L). The final resultant water solution was passed through a weak basic ion-exchange resin (D301T, Nankai University Chemical Plant) with water as mobile phase to remove the remaining  $\text{HCl}$  acid. Then water was removed through a drying process for the collected water solution to yield 3.5 g of product.

In a typical experiment, GO (40 mg) dispersed in ethanol ( $\geq 99\%$ ) was sonicated for 2 h, then 1.352 g  $\text{FeCl}_3 \cdot 6\text{H}_2\text{O}$  (Sinopharm Chemical Reagent Corp.,  $\geq 99\%$ ) was added to GO solution with a trace addition of deionized water (3.5 mL) under vigorous stirring for 30 min, 4 g sodium acetate (Sinopharm Chemical Reagent Corp.,  $\geq 99\%$ ) was added to the mixture solution for another 1 h stirring. Then the mixture was transferred to a Teflon-lined autoclave (100 mL) and followed by hydrothermal treatment at 180  $^\circ\text{C}$  for 24 h. Following natural cooling to ambient temperature, the samples were collected by centrifugation, and washed with deionized water and ethanol three times, respectively. The obtained products were dried in the oven at 60  $^\circ\text{C}$  for 6 h for characterization. The  $\alpha$ - $\text{Fe}_2\text{O}_3$ /graphene composites with different weight ratios of GO to  $\alpha$ - $\text{Fe}_2\text{O}_3$  were synthesized by adjusting the addition contents of GO. The compared pure  $\alpha$ - $\text{Fe}_2\text{O}_3$  nanoplates were prepared by the same procedure without the introduction of GO.<sup>[31]</sup>

The photocatalytic performances of all the obtained samples were measured toward degradation of RhB under Xe light (350 W) irradiation at room temperature, and the degradation of Rhodamine B (RhB) was observed based on the absorption spectroscopic technique. Typically, 30 mg of the photocatalysts were added to the Rhodamine B solution (10 mg/L) with 0.7 mL H<sub>2</sub>O<sub>2</sub> (≥30 wt%). The reaction mixture was stirred in the dark for 40 min to achieve the adsorption-desorption equilibrium between RhB and the photocatalyst, then the solution was exposed to the Xe light irradiation under ambient conditions with the constant stirring. After given time intervals, the mixture solution was centrifuged and analyzed by measuring the absorbance of RhB at 550 nm.<sup>[53]</sup>

The prepared α-Fe<sub>2</sub>O<sub>3</sub> nanoplates and α-Fe<sub>2</sub>O<sub>3</sub>/graphene composites with different weight ratios of GO were characterized using X-ray diffraction using Cu Kα radiation (XRD, Bruker D8-A25), field-emission scanning electron microscope (FESEM, JSM-6701F), transmission electron microscope (TEM, CM200FEG), and atomic force microscopy (AFM, Bruker Dimension Icon). After the structural and chemical examinations, the absorption and fluorescence spectras of the samples were taken at room temperature with a UV-visible spectrophotometer (Hitachi U-4100), and the photoluminescence (PL) spectrofluorometer (Fluoromax-4) with an excitation at 350 nm light. The XPS spectras were collected by a Perkin Elmer PHI 5000 C ESCA system equipped with a hemispherical electron energy analyzer. The Mg-Kα (1253.6 eV) anode was operated at 14 kV and 20 mA. The FT-IR and Raman spectras were recorded on Nexus 470 FT-IR spectrometer and Spex 403 Raman spectrometer. And BET surface area and pore size were conducted by nitrogen adsorption-desorption method at 77K (Micromeritics Tristar ASAP 3000).

## Acknowledgements

This work was supported by the Science and Technology Commission of Shanghai Municipality (13NM1400300), Shanghai Shu Guang Project (12SG01), National Natural Science Foundation of China (Grant Nos. 91123006 and 51372040), Shanghai Pujiang Program (12PJ1400300), Innovation Program of Shanghai Municipal Education Commission (14ZZ003), the Programs for Professor of Special Appointment (Eastern Scholar) at Shanghai Institutions of Higher Learning and for New Century Excellent Talents in University (NCET-11-0102).

Received: April 21, 2014

Revised: May 14, 2014

Published online: July 14, 2014

- [1] W. W. Zhou, C. W. Cheng, J. P. Liu, Y. Y. Tay, J. Jiang, X. T. Jia, J. X. Zhang, H. Gong, H. H. Hng, T. Yu, H. J. Fan, *Adv. Funct. Mater.* **2011**, *21*, 2439.
- [2] J. S. Chen, T. Zhu, X. H. Yang, H. G. Yang, X. W. Lou, *J. Am. Chem. Soc.* **2010**, *132*, 13162.
- [3] Z. Y. Fan, X. G. Wen, S. H. Yang, J. G. Lu, *Appl. Phys. Lett.* **2005**, *87*, 013113.
- [4] X. S. Fang, Y. Bando, U. K. Gautam, C. H. Ye, D. Golberg, *J. Mater. Chem.* **2008**, *18*, 509.
- [5] Z. Sun, H. Yuan, Z. Liu, B. Han, X. Zhang, *Adv. Mater.* **2005**, *17*, 2993.
- [6] H. Katsuki, S. Komarneni, *J. Am. Ceram. Soc.* **2003**, *86*, 183.
- [7] K. Sivula, R. Zboril, F. Le Formal, R. Robert, A. Weidenkaff, J. Tucek, J. Frydrych, M. Gratzel, *J. Am. Chem. Soc.* **2010**, *132*, 7436.
- [8] C. Jorand Sartoretto, B. D. Alexander, R. Solaraska, I. A. Rutkowska, J. Augustynski, R. Cerny, *J. Phys. Chem. B* **2005**, *109*, 13685.
- [9] J. Z. Zhang, *J. Phys. Chem. B* **2000**, *104*, 7239.
- [10] M. Zhang, Y. Lin, T. J. Mullen, W. F. Lin, L. D. Sun, C. H. Yan, T. E. Patten, D. Wang, G. Y. Liu, *J. Phys. Chem. Lett.* **2012**, *3*, 3188.
- [11] W. Cheng, J. He, Z. Sun, Y. Peng, T. Yao, Q. Liu, Y. Jiang, F. Hu, Z. Xie, B. He, *J. Phys. Chem. C* **2012**, *116*, 24060.
- [12] A. J. Frierdich, M. M. Scherer, J. E. Bachman, M. H. Engelhard, B. W. Rapponotti, J. G. Catalano, *Environ. Sci. Technol.* **2012**, *46*, 10031.
- [13] H. Chang, H. K. Wu, *Adv. Funct. Mater.* **2013**, *23*, 1984.
- [14] Y. H. Ng, I. V. Lightcap, K. Goodwin, M. Matsumura, P. V. Kamat, *J. Phys. Chem. Lett.* **2010**, *1*, 2222.
- [15] L. W. Zhang, H. B. Fu, Y. F. Zhu, *Adv. Funct. Mater.* **2008**, *18*, 2180.
- [16] Y. Zhang, N. Zhang, Z. R. Tang, Y.-J. Xu, *Phys. Chem. Chem. Phys.* **2012**, *14*, 9167.
- [17] O. Akhavan, E. Ghaderi, *J. Phys. Chem. C* **2009**, *113*, 20214.
- [18] Y. Zhang, Z. R. Tang, X. Fu, Y. J. Xu, *ACS Nano* **2010**, *4*, 7303.
- [19] L. He, L. Jing, Z. Li, W. Sun, C. Liu, *RSC Adv.* **2013**, *3*, 7438.
- [20] L. Xiao, D. Wu, S. Han, Y. Huang, S. Li, M. He, F. Zhang, X. Feng, *ACS Appl. Mater. Interfaces* **2013**, *5*, 3764.
- [21] S. Y. Liu, J. Xie, Q. Pan, C. Y. Wu, G. S. Cao, T. J. Zhu, X. B. Zhao, *Int. J. Electrochem. Sci.* **2012**, *7*, 354.
- [22] J. Zhu, T. Zhu, X. Zhou, Y. Zhang, X. W. Lou, X. Chen, H. Zhang, H. H. Hng, Q. Yan, *Nanoscale* **2011**, *3*, 1084.
- [23] G. K. Pradhan, D. K. Padhi, K. Parida, *ACS Appl. Mater. Interfaces* **2013**, *5*, 9101.
- [24] H. Li, Q. Zhao, X. Li, Z. Zhu, M. Tade, S. Liu, *J. Nanoparticle Res.* **2013**, *15*, 1.
- [25] J. W. Seo, J. t. Jang, S. w. Park, C. Kim, B. Park, J. Cheon, *Adv. Mater.* **2008**, *20*, 4269.
- [26] S. A. Morin, A. Forticaux, M. J. Bierman, S. Jin, *Nano Lett.* **2011**, *11*, 4449.
- [27] S. Z. Butler, S. M. Hollen, L. Cao, Y. Cui, J. A. Gupta, H. R. Gutierrez, T. F. Heinz, S. S. Hong, J. Huang, A. F. Ismach, *ACS Nano* **2013**, *7*, 2898.
- [28] A. Ye, W. Fan, Q. Zhang, W. Deng, Y. Wang, *Catal. Sci. Technol.* **2012**, *2*, 969.
- [29] C. Xu, X. Wang, J. Zhu, X. Yang, L. Lu, *J. Mater. Chem.* **2008**, *18*, 5625.
- [30] J. Liu, H. Bai, Y. Wang, Z. Liu, X. Zhang, D. D. Sun, *Adv. Funct. Mater.* **2010**, *20*, 4175.
- [31] L. Chen, X. Yang, J. Chen, J. Liu, H. Wu, H. Zhan, C. Liang, M. Wu, *Inorg. Chem.* **2010**, *49*, 8411.
- [32] G. Titelman, V. Gelman, S. Bron, R. Khalfin, Y. Cohen, H. Bianco-Peled, *Carbon* **2005**, *43*, 641.
- [33] M. S. A. S. Shah, K. Zhang, A. R. Park, K. S. Kim, N. G. Park, J. H. Park, P. J. Yoo, *Nanoscale* **2013**, *5*, 5093.
- [34] H. Liu, G. Shao, J. Zhao, Z. Zhang, Y. Zhang, J. Liang, X. Liu, H. Jia, B. Xu, *J. Phys. Chem. C* **2012**, *116*, 16182.
- [35] D. Lin, H. Wu, R. Zhang, W. Pan, *Chem. Mater.* **2009**, *21*, 3479.
- [36] Y. T. Liang, B. K. Vijayan, K. A. Gray, M. C. Hersam, *Nano Lett.* **2011**, *11*, 2865.
- [37] Y. Zhang, Z. R. Tang, X. Fu, Y. J. Xu, *ACS Nano* **2011**, *5*, 7426.
- [38] W. Wang, J. Yu, Q. Xiang, B. Cheng, *Appl. Catal. B: Environ.* **2012**, *119*, 109.
- [39] R. Nair, P. Blake, A. Grigorenko, K. Novoselov, T. Booth, T. Stauber, N. Peres, A. Geim, *Science* **2008**, *320*, 1308.
- [40] N. Yang, Y. Liu, H. Wen, Z. Tang, H. Zhao, Y. Li, D. Wang, *ACS Nano* **2013**, *7*, 1504.
- [41] M. R. Hoffmann, S. T. Martin, W. Y. Choi, D. W. Bahnemann, *Chem. Rev.* **1995**, *95*, 69.
- [42] M. Pelaez, N. T. Nolan, S. C. Pillai, M. K. Seery, P. Falaras, A. G. Kontos, P. S. Dunlop, J. W. Hamilton, J. A. Byrne, K. O'Shea, *Appl. Catal. B: Environ.* **2012**, *125*, 331.
- [43] K. K. Haldar, G. Sinha, J. Lahtinen, A. Patra, *ACS Appl. Mater. Interfaces* **2012**, *4*, 6266.
- [44] X. Xing, R. Liu, X. Yu, G. Zhang, H. Cao, J. Yao, B. Ren, Z. Jiang, H. Zhao, *J. Mater. Chem. A* **2013**, *1*, 1488.

- [45] Y. Shi, H. Li, L. Wang, W. Shen, H. Chen, *ACS Appl. Mater. Interfaces* **2012**, *4*, 4800.
- [46] H. I. Kim, G.-h. Moon, D. Monllor-Satoca, Y. Park, W. Choi, *J. Phys. Chem. C* **2011**, *116*, 1535.
- [47] J. Paredes, S. Villar-Rodil, M. Fernández-Merino, L. Guardia, A. Martínez-Alonso, J. Tascón, *J. Mater. Chem.* **2011**, *21*, 298.
- [48] S. C. Han, L. F. Hu, N. Gao, A. A. Al-Ghamdi, X. S. Fang, *Adv. Funct. Mater.* **2014**, *24*, 3725.
- [49] S. Guo, G. Zhang, Y. Guo, J. C. Yu, *Carbon* **2013**, *60*, 437.
- [50] J. Bacardit, J. Stötzner, E. Chamarro, S. Esplugas, *Ind. Eng. Chem. Res.* **2007**, *46*, 7615.
- [51] M. Hirata, T. Gotou, S. Horiuchi, M. Fujiwara, M. Ohba, *Carbon* **2004**, *42*, 2929.
- [52] H. A. Becerril, J. Mao, Z. F. Liu, R. M. Stoltenberg, Z. N. Bao, Y. S. Chen, *ACS Nano* **2008**, *2*, 463.
- [53] H. S. Wu, L. D. Sun, H. P. Zhou, C. H. Yan, *Nanoscale* **2012**, *4*, 3242.
-